Determination of dopant site occupancies in Cu-substituted $YBa_2Cu_3O_{7-\delta}$ by differential anomalous x-ray scattering

R. S. Howland and T. H. Geballe
Department of Applied Physics, Stanford University, Stanford, California 94305

S. S. Laderman, A. Fischer-Colbrie, and M. Scott
Hewlett-Packard Company, 3500 Deer Creek Rd., Palo Alto, California 94304

J. M. Tarascon and P. Barboux
Bell Communications Research, 331 Newman Springs Rd. Red Bank, New Jersey 07701
(Received 19 December 1988)

Dopant site occupancies in $YBa_2Cu_{3-x}M_xO_{7-\delta}$, with M=Fe (x=0.3 and x=0.5), Co (x=0.2 and x=0.5), Ni (x=0.3), and Zn (x=0.3) have been found using differential anomalous x-ray scattering. The Ni and Zn atoms were found to occupy the Cu(1) ("chains") site and the Cu(2) ("planes") site in a nearly random distribution. The Fe and Co atoms were found to occupy the Cu(1) site predominantly at low x, with an increasing fraction on the Cu(2) sites as the total amount of dopant increases. In all cases, our results appear to have high statistical significance, with very little sensitivity to expected uncertainties in oxygen content, total dopant content, anomalous corrections to the atomic scattering factor of the dopant, and to relative atomic coordinates assumed in the modeling. We have also discussed the results in the context of existing extended x-ray-absorption fine-structure and neutron-diffraction results, thermogravimetric analysis, Mössbauer spectra, and T_c and Hall-effect studies.

INTRODUCTION

Research to date has indicated that the presence of copper oxide layers is essential for superconductivity above 90 K. In the most widely studied superconductor of this class, $YBa_2Cu_3O_{7-\delta}$, two crystallographically distinct Cu-O environments are present. The six-layer unit cell is composed of a Cu(1)-O layer sandwiched between Ba-O layers, stacked on top of Cu(2)-O layers separated by a Y layer.[1-7] Within the orthorhombic structure, the Cu(1) or "chains" site has four nearest neighbors of oxygen in a nearly square-planar conformation, while the two Cu(2) or "planes" sites have five nearest neighbors of oxygen in a nearly square-pyramidal configuration. The two sites are considered to play distinctly different roles in determining the physical properties of the material. By examining the correlation between changes in the physical properties with transition-metal substitutions, the roles of the two Cu sites may become clear. Such studies rely upon accurate determinations of the positions of the dopants within the unit cell. In this paper, we present Cu-site occupancies for Co, Fe, Ni, and Zn determined by anomalous x-ray scattering. Unlike neutron scattering data, the x-ray determinations presented here appear to have high accuracy in every case. Our results are discussed with respect to complementary structural determinations [neutron scattering and extended x-ray-absorption fine-structure (EXAFS)], studies of local chemistry (Mössbauer), and macroscopic physical properties [thermogravimetric analysis (TGA), T_c, and Hall effect]. Some of these studies used samples virtually identical to those used here, and thus the results can be compared directly.

EXPERIMENT

Differential anomalous x-ray scattering (DAS) is a diffraction technique that takes advantage of the variation of the scattering cross section of an atom at energies near its x-ray-absorption edge.[8] In our experiment synchrotron radiation is tuned to energies near the absorption edge of the dopant, changing its atomic scattering factor. Because only one atomic species changes its scattering factor appreciably, contributions involving that atom can be distinguished. DAS is a differential process, in that changes in intensity with energy are utilized. This approach is markedly different from experiments based on the analysis of scattering data at a single energy. We have found that for certain questions, such as those posed here, this method has the potential to lead to better convergence.

In order to select appropriate samples and reflections to study, we calculated the variation in intensity of the allowed peaks with energy for energies near the x-ray-absorption edge of the dopants, and the dependence of that variation upon the distribution of dopant atoms within the unit cell. Since we were interested primarily in distinguishing between the Cu(1) and Cu(2) sites, and not the ordering of the dopants within these sites, we distributed the dopant atoms randomly within the a-b planes for a given site. We then selected two reflections whose simulated differential intensities show maximum sensitivity to the distribution of dopant atoms over the sites, the (001) and (004) peaks, and two "control" reflections whose intensities were minimally sensitive to the distribution of the dopant atoms, the (003) and (113) peaks. Because the lattice constants change with doping, the (100)

and/or the (010) peaks can overlap with the (003) peak. The overlap was taken into account, but since neither the energy dependences nor the sensitivities to dopant distribution differ significantly among the three reflections, these corrections are smaller than our experimental precision. Henceforth we shall refer to this peak as (003) for simplicity. The simulations also allowed us to estimate the minimum dopant concentration detectable by this technique, about $x=0.1$, assuming changes in intensities can be measured to an accuracy of about 2%. We selected six samples of transition-metal doped $YBa_2Cu_{3-x}M_xO_{7-\delta}$: M=Ni ($x=0.3$), Zn ($x=0.3$), Fe ($x=0.3$), Fe ($x=0.5$), Co ($x=0.2$), and Co ($x=0.5$).

The samples used in this experiment are bulk powders prepared by solid-state reaction, identical to those described in an earlier paper.[9] Lattice constants, superconducting transition temperatures, and oxygen contents are listed in that work. In summary, the Ni- and Zn-doped samples are orthorhombic and superconducting at a depressed T_c, while the Fe- and Co-doped samples are superconducting at a depressed T_c at the lower dopant concentration and nonsuperconducting at the higher dopant concentration. All the Fe- and Co-doped samples studied are tetragonal. X-ray powder-diffraction scans show that the Ni- and Zn-doped samples, doped to their maximum solubility,[9] are slightly contaminated with $Y_2Ba[Cu,Ni]O_5$ and possibly with $Ba[Cu,Ni]O_2$, but our analysis is not affected by the contamination except where diffraction peaks of the contaminating phase overlap $YBa_2Cu_3O_{7-\delta}$ reflections. Such an overlap occurs in the case of the (004) and (113) peaks of the Ni- and Zn-doped samples, and these data are discarded.

Successful comparison of intensities in a powder-diffraction experiment depends upon the assumption of a random distribution of illuminated grains. The high collimation of synchrotron radiation makes this condition more difficult to achieve than in a conventional x-ray-diffraction experiment. The special problems of powder diffraction using synchrotron radiation have been documented in the literature.[10] Our simulations demonstrated that merely to distinguish the limiting cases of all dopants on the Cu(1) site from all dopants on the Cu(2) site requires a knowledge of the intensities to about $\pm 10\%$ for a dopant level of $x=0.5$. We aimed for an accuracy of 2%.

To increase the effective number of grains sampled we took three steps: grinding the powder to a grain size of 10 μm or less, as measured by scanning electron microscopy; rotating the sample about an axis perpendicular to the sample's surface; and employing θ scans to estimate the intensity more accurately, as described below. Deviation from random orientation was evaluated by examining the scans of θ, the coaxial inner circle of the two-circle diffractometer, with 2θ fixed at the diffraction peak (Fig. 1). The θ scan of a truly random powder should be smooth with very low variance arising strictly from counting noise. The variance then indicates the accuracy with which the intensity can be estimated. In our experiment, θ was scanned 1° on each side of the systematic condition, in steps of 0.02°, for a total of 100 measurements of the peak intensity. We found that asymmetric absorption and slit corrections contributed shape to the θ scans, particularly for the (001) reflections. For the small energy changes used here, the energy dependence of such geometric factors is negligible. When these effects are removed, our θ scans are flat and display a standard deviation in intensity of roughly 2%.

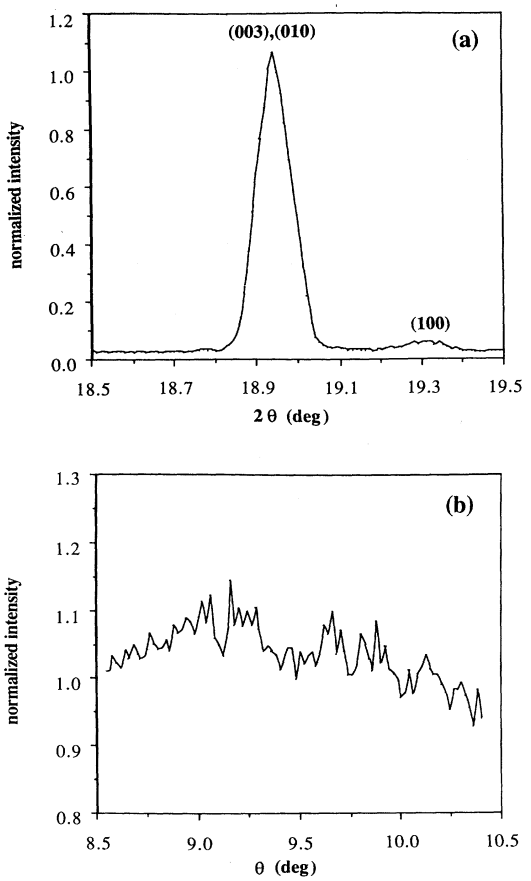

FIG. 1. (a) Symmetric θ-2θ and (b) θ scans of the (003) peak of the Zn ($x=0.3$) sample, at 9657 eV. The θ scans were collected with 2θ set to the diffraction condition. The intensity of the elastic signal is normalized by the incident intensity in both cases.

Intensities were measured as a function of energy at the Stanford Synchrotron Radiation Laboratory, at the Beam Line IV-3 Powder Diffraction Station, with ring operating conditions of 3 GeV and 35 mA, and a wiggler field of 18 kG. Our only significant modification to the standard two-circle diffractometer was the attachment of a small spinning motor to the inner circle for rotation of the sample, as described above, at a rate of 1 Hz. The powders were packed into the wells of glass slides to a depth of about 2 mm, much greater than the penetration depth of the x rays at these energies. While the most of the beam path was filled with helium, the sample itself was in air. The length of the total beam path in air was 5.7 cm. Entrance and exit slits measured 0.6×8.0 mm^2.

Energy calibration was accomplished with near-edge scans of EXAFS samples from the same powders. One of the dopant K edges was measured each time the storage

ring was injected with electrons. In addition, detailed energy scans, 1000 eV on either side of the dopant K edge, were collected to enable accurate calculations of the anomalous corrections to the atomic structure factors of the dopants. For this work, we have defined the K edge as the energy at which absorption reaches half its maximum value.

For each sample, 32 diffraction scans were taken: a symmetric θ-2θ scan, and a θ scan with 2θ fixed at its peak, at each of four energies, for each of four reflections. The (001), (003), (004), and (113) peaks were scanned at energies 70, 10, 5, and 0 eV below the dopant K edge for the Fe-, Co-, and Zn-doped samples, and 65, 5, and 0 eV below and 5 eV above the K edge for the Ni-doped sample. Due to limited time, the (113) reflection was not studied for the Co ($x=0.2$) sample, and the second and fourth energies of the (004) peak were also not measured. For the same reason, the intensities of the (001) and (113) reflections of the Ni-doped sample were not measured at the highest energy.

ANALYSIS

Extraction of relative intensities from the data involves both θ-2θ and θ scans. The θ-2θ scan is used to determine the background intensity, while the intensity of the Bragg peak is derived from the θ scan. If the θ scan were flat with variance arising from counting noise only, the relative intensity of the reflection at the energy could be defined as the ratio of the mean of the θ scan divided by (for example) the mean of the lowest-energy θ scan. However, the θ scans of our experiment contain geometric factors that contribute curvature, as well as "noise" arising from the small number of grains illuminated by the beam, in addition to the standard photon-counting noise. We decided to apply the observation that the four energies of a given reflection for a given sample have virtually identical geometric factors, and assume that all reproduce the "noise" contributed by the individual grains. Thus we calculated the relative intensities by superimposing each θ scan on the lowest-energy θ scan via a least-squares fit. The scale factor that produces the best fit becomes the relative intensity of that θ scan to the lowest-energy θ scan. In this way, we have divided out the geometric contributions and the structure arising from individual grains. Then the dominant source of noise remaining in the θ scans is photon-counting noise.

When all four θ scans are scaled and superimposed, an average intensity can be computed at each point, and the standard deviation of the individual θ scans from this average scan should reflect the accuracy with which the relative intensity is estimated. These are the standard deviations used in the computation of the R value, described below, and they also appear as the error bars in Figs. 3 through 8.

Once the relative intensities are extracted from the data, they can be compared with the calculated energy dependence of peak intensities as a function of the distribution of the dopant atoms between the two Cu sites. However, experimental values are now used to improve the model calculations. Instead of theoretical free-atom values of the anomalous corrections to the atomic structure factors of the dopants, experimental values which incorporate the solid-state effects of the dopant's local environment in Y-Ba-Cu-O can be calculated from the detailed EXAFS scans of the dopant's K edges.[11] As an example, $f'(E)$ and $f''(E)$, which are extracted from the Co K-edge scan, are given for Co in Figs. 2(a) and 2(b). These values are used directly in the model calculation. For the other elements (Y, Ba, Cu, O) theoretical atomic values for $f'(E)$ and $f''(E)$ are used, as in the *a priori* simulations.[12] For these atoms use of the free-atom values is warranted because the energy ranges in the experiment are far from their x-ray-absorption edges.

Once $f''(E)$ is calculated for each atom, corrections for absorption in the sample can be made more accurately. In addition, small corrections for the energy dependence of the air scatter in the vicinity of the sample as well as that of the Kapton windows sealing the beam path were made. Finally, the contribution of the nonlinearity of the

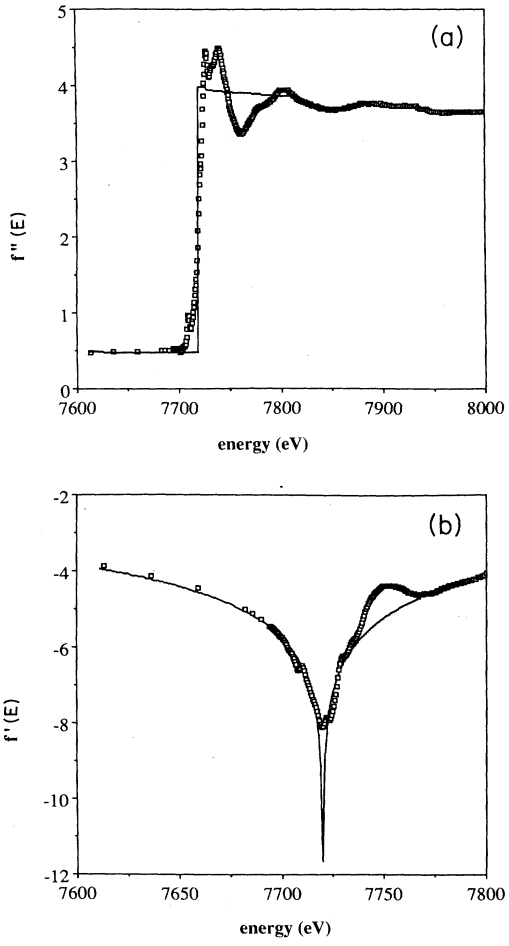

FIG. 2. (a) The imaginary part of the correction to the atomic scattering factor of Co, as a function of energy. (b) The real part of the correction to the atomic scattering factor of Co as a function of energy. $f'(E)$ is calculated from $f''(E)$. In both (a) and (b), solid lines represent theoretical, free-atom values, while small squares represent values derived from absorption scans.

incident-beam detector with energy was included in the models.

Intensity as a function of energy was calculated for each sample and each of the reflections, assuming a fraction of the dopant atoms x_1 on the Cu(1) site and the remaining dopant atoms, $x_2 = 1 - x_1$, divided equally between the two Cu(2) sites. While the lattice parameters and oxygen concentrations were taken from direct measurements,[9] the relative atomic coordinates for the models were based on neutron powder-diffraction measurements of comparable samples, when available, or on the relative coordinates of the undoped material[3] otherwise. Thus, for the Co-doped samples, relative coordinates were taken from neutron studies of samples nearly identical to ours,

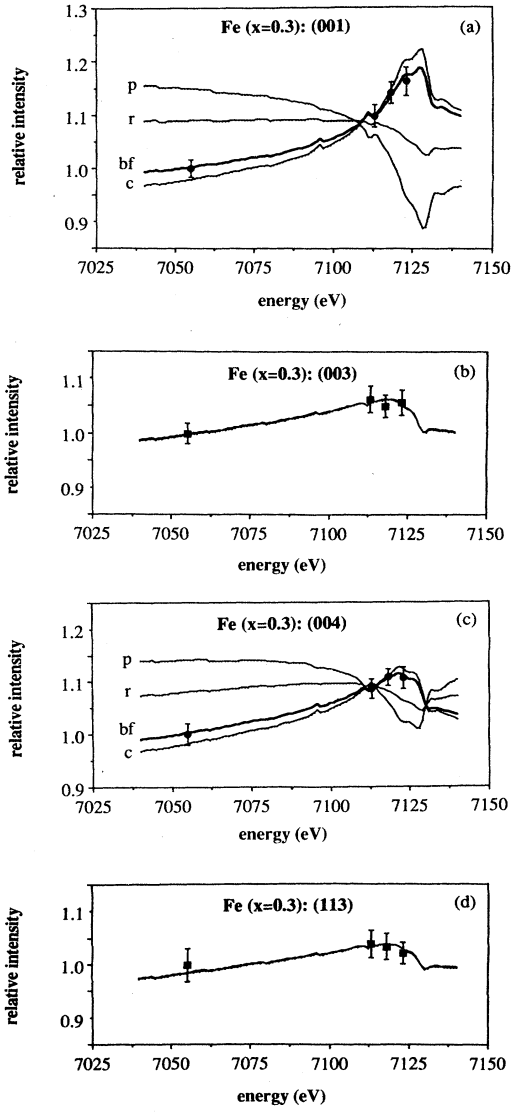

FIG. 3. The variation of the relative intensity of various peaks as a function of energy for the Fe ($x = 0.3$) sample. Error bars represent one standard deviation in the data sets and are described more fully in the text. The calculated variation of the intensity for the best-fit model is shown with solid line and labeled bf; the $x_1 = 1.0$ (all chains) model is labeled c, the $x_1 = 0.33$ (random) model is labeled r, and the $x_1 = 0.00$ (all planes) model is labeled p. (a) The (001) peak. (b) The (003) peak. Because this peak is insensitive to the distribution of the dopant atoms within the unit cell, only the $x_1 = 0.00$ and $x_1 = 1.00$ models are shown. They overlap almost entirely. (c) The (004) peak. (d) The (113) peak with the $x_1 = 0.00$ and $x_1 = 1.00$ models.

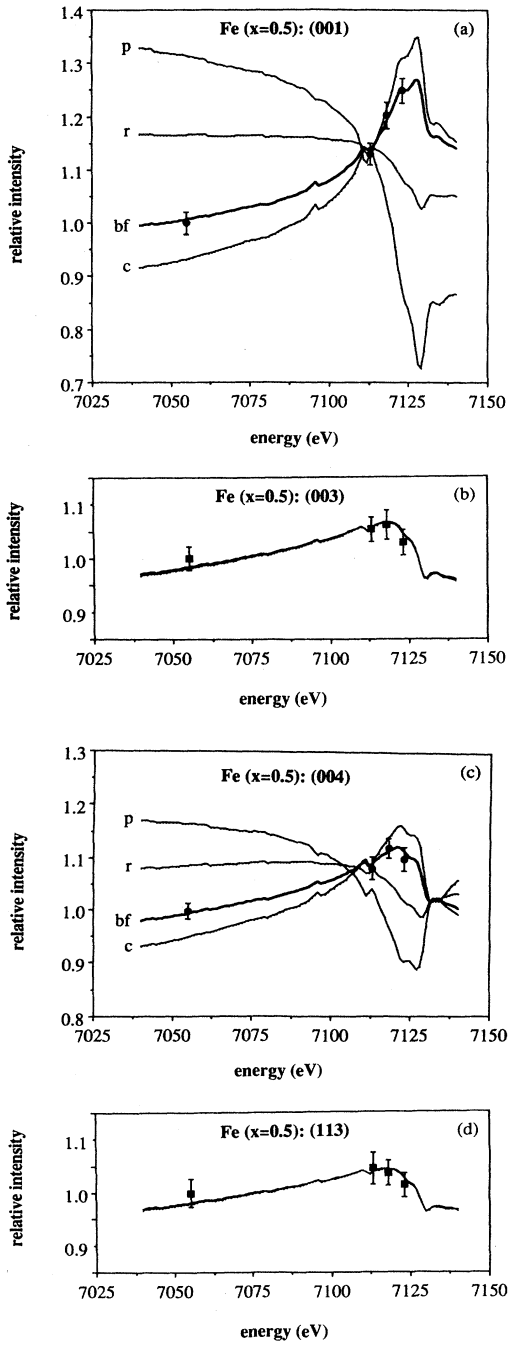

FIG. 4. The variation of the relative intensity of various peaks as a function of energy, for the Fe ($x = 0.5$) sample. Error bars and calculated models as in Fig. 3. (a) The (001) peak. (b) The (003) peak. (c) The (004) peak. (d) The (113) peak.

Y-Ba-Cu-O doped with Co to $x=0.2$ and $x=0.8$.[13] For our Co ($x=0.2$) model the coordinates were used directly, whereas interpolated coordinates were used for Co ($x=0.5$) model. For our Zn ($x=0.3$) model, coordinates were extrapolated from the neutron powder data of a Zn ($x=0.18$) sample.[14] The undoped coordinates were used for the Ni-doped sample because preliminary neutron studies have demonstrated that Ni doping does little to change the relative positions of the atoms in the unit cell.[13] Three sets of relative coordinates were available for Fe-doped Y-Ba-Cu-O, one based on a Rietveld analysis of x-ray-diffraction data[15] and the others based on neutron powder diffraction.[16,17] Unfortunately, all of these studies used samples with c-axis lattice parameters much different from ours, and we elected to use the undoped relative coordinates instead, because they matched the c axis of our Fe-doped samples more closely. The effects of imposing the doped coordinates upon our Fe-doped samples are examined in more detail in the last paragraph of the Results section. We note that in principle the relative coordinates could have been obtained from Rietveld analysis of our data if more reflections had been collected.

For the tetragonal samples, the distribution of O atoms within the Cu(1) plane was also made tetragonal: The oxygens were distributed equally in the a and b directions, thus disrupting the "chains." However, the dopant site distributions are derived from (001) and (004) reflections, which are insensitive to the oxygen distribution within the a-b planes.

For a given sample and dopant distribution x_1 (x_2 is fixed to $1-x_1$), the energy dependence of the calculated relative intensity of each reflection is compared with that of the data, and the fit is evaluated by calculating $R_{hkl}(x_1)$:

$$R_{hkl}(x_1)=\sum_{i=1}^{4}\frac{[I_i^{\text{data}}-\alpha_{hkl}(x_1)I_i^{\text{model}}(x_1)]^2}{\sigma_i^2},$$

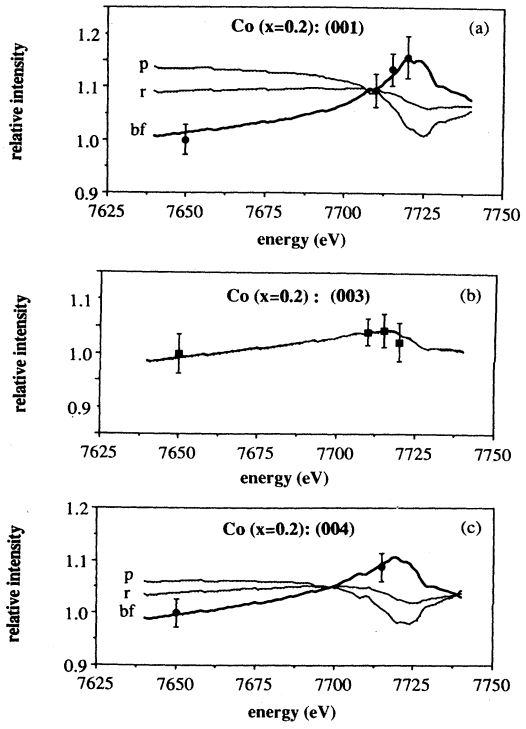

FIG. 5. The variation of the relative intensity of various peaks as a function of energy, for the Co ($x=0.2$) sample. Error bars and calculated models as in Fig. 3. (a) The (001) peak. (b) The (003) peak. (c) The (004) peak. No (113) data were collected for the Co ($x=0.2$) sample.

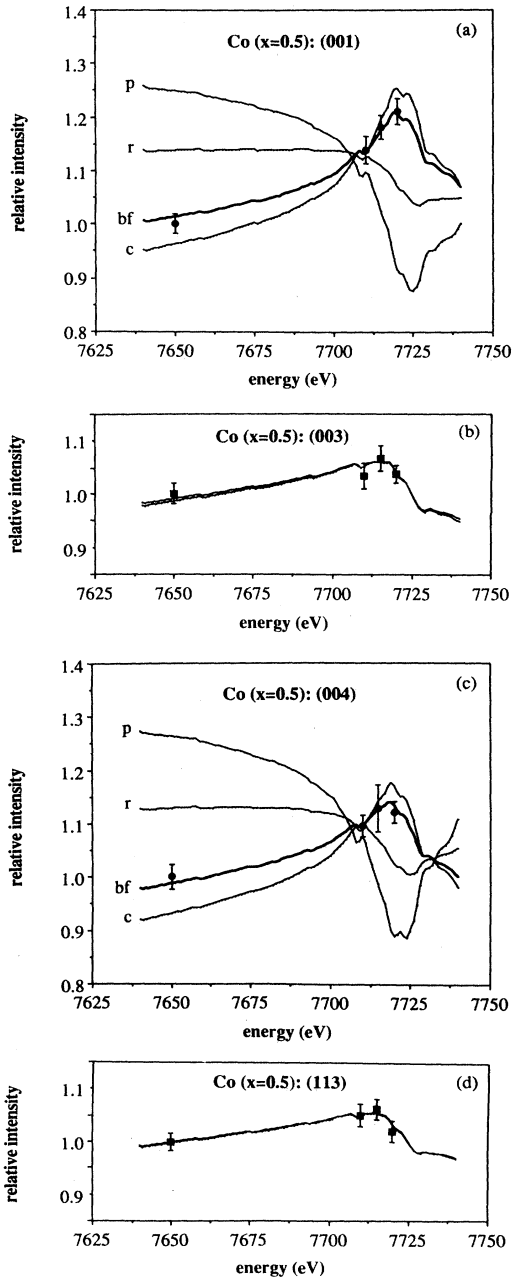

FIG. 6. The variation of the relative intensity of various peaks as a function of energy, for the Co ($x=0.5$) sample. Error bars and calculated models as in Fig. 3. (a) The (001) peak. (b) The (003) peak. (c) The (004) peak. (d) The (113) peak.

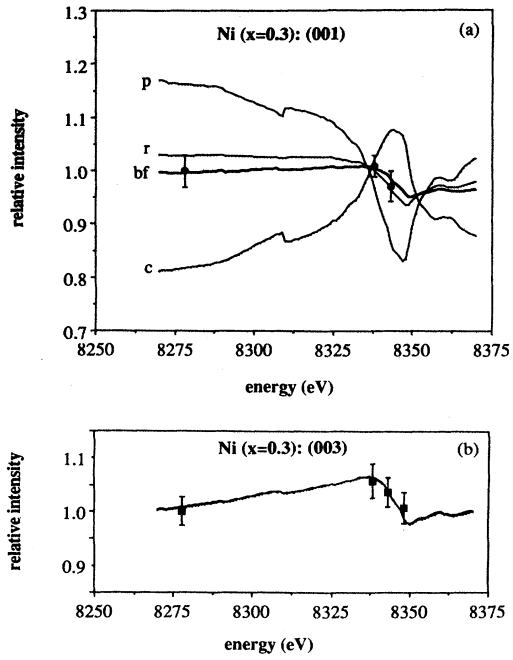

FIG. 7. The variation of the relative intensity of various peaks as a function of energy, for the Ni ($x=0.3$) sample. Error bars and calculated models as in Fig. 3. (a) The (001) peak. (b) The (003) peak. The data collected for the (004) and (113) peaks of the Ni-doped sample were contaminated with Y_2BaCuO_5.

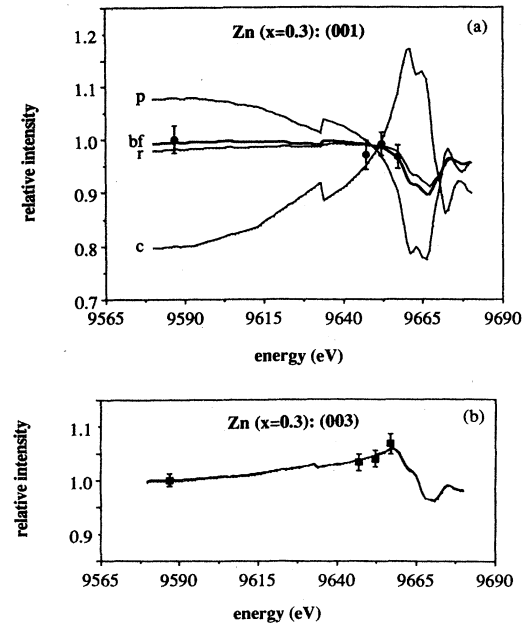

FIG. 8. The variation of the relative intensity of various peaks as a function of energy, for the Zn ($x=0.3$) sample. Error bars and calculated models as in Fig. 3. (a) The (001) peak. (b) The (003) peak. The data collected for the (004) and (113) peaks of the Zn-doped sample were contaminated with Y_2BaCuO_5.

where α_{hkl} is the scale factor of reflection (hkl), found by a least-squares fit of the relative intensities I_i of the models to the data, the σ_i are the standard deviations in peak intensity described above, and the sum is over the four energies at which data were collected. The introduction of α_{hkl} is necessary to set the relative scale between the data and the model. Because the differential intensities of the (003) and (113) reflections are insensitive to the distribution of the dopant between the Cu sites, $R_{003}(x_1)$ and $R_{113}(x_1)$ are relatively flat. In contrast, $R_{001}(x_1)$ and $R_{004}(x_1)$ show signficant curvature with well-defined minima which give estimates of the best-fit value of x_1. The final estimate of the best-fit value of x_1 is given by the minimum of the sum $R(x_1)=R_{001}(x_1)+R_{004}(x_1)$. In Figs. 3 through 8, the energy variations of the four

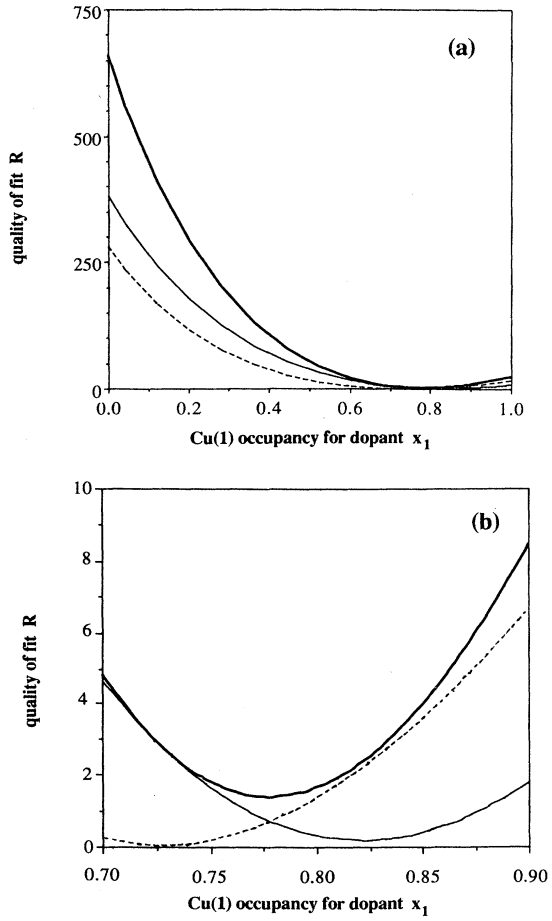

FIG. 9. The variation of the quality of fit R with the fractional dopant concentration x_1 for the Co ($x=0.5$) sample. (a) The entire range of x_1 from $x_1=0.00$ (all planes) to $x_1=1.00$ (all chains), for the (001) (solid line) and (004) (dashed line) peaks, and their sum (heavy and solid line). (b) A closeup of the best-fit region for the (001) and (004) peaks and their sum [line types as in (a)]. For the (003) and (113) peaks, $R(x_1)$ is indistinguishable from the horizontal axis because of its small magnitude and insensitivity to the distribution of the dopant atoms within the unit cell. The other five samples all show better agreement between the (001) and (004) minima as listed in Table I.

reflections are shown with the $x_1=0.0$, 0.33, 1.0, and best-fit models for the six samples. In Fig. 9 the variations of R_{001}, R_{004}, and R with x_1 are shown for the Co ($x=0.5$) sample, (a) over the full range of x_1 and (b) in the neighborhood of the best-fit values. Note that the (001) and (004) curves have minima slightly displaced, but for all samples this displacement is small enough that the error bar assigned to the (001)-determined value of x_1 always overlaps the error bar assigned to the (004)-determined value of x_1. (The assignment of error bars to x_1 is described in the next paragraph.) Note also that the (001) curve dominates the sum R because it is the more sensitive to the relative positions of the dopants. The high curvature of $R(x_1)$ is indicative of good statistical significance: in Fig. 9, the data fits $x_1=0.78$ with an R value 16 times better than the $x_1=1.0$ (all chains), 464 times better than the $x_1=0.0$ (all planes) models, and a factor of 110 better than the $x_1=0.33$ (random) model. Comparisons of the R values for fits to the three limiting models with those of the best-fit models appear in Table II.

The uncertainty in the best-fit value of x_1 is estimated by applying a reduced χ^2 test. In this test, R, which is also χ^2, is divided by the number of degrees of freedom (the number of data points minus the number of fitting parameters), and a 95% confidence level is computed from a standard table.[18] The applicability of this standard statistical method is difficult to test with such a small number of data points. However, this test does have the following convincing properties: (1) error bars are smaller when $R(x_1)$ has higher curvature, meaning that deviations from the best-fit value cause the quality of fit to worsen rapidly; (2) error bars are sensitive to the magnitude of R, i.e., the quality of fit, and to the number of degrees of freedom in the fit; (3) error bars determined from the sum $R=R_{001}+R_{004}$ are inversely proportional to the agreement between the (001) and (004) results; and (4) error bars of x_1 are roughly in agreement with the error bars of Figs. 3 through 8, in that the range of x_1 that encompasses its error bar would produce models whose intensities lie within the relative-intensity error bars that arose from the standard deviations of the θ scans.

RESULTS

The resulting optimal dopant site occupancies and their uncertainties are listed in Table I and displayed graphically in Fig. 10. We have demonstrated, with good statistical significance, that Ni and Zn dopants are distributed roughly equally among the Cu sites. [An equal distribution over the Cu sites would give $x_1=0.33$, since twice as many Cu(2) sites are present in the unit cell.] Fe and Co dopants, on the other hand, preferentially occupy the Cu(1) site, with increasing occupation of the Cu(2) site as x increases.

The statistical significance of these results is evident in the agreement between the (001) and (004) results for a given sample and in the high curvature of $R(x_1)$ of Fig. 9 and Table II. However, these criteria do not take into account systematic uncertainties due to uncertainties in oxygen concentration, total dopant concentration, anomalous corrections to the atomic scattering factors of the dopant, and relative atomic coordinates.

TABLE I. Best-fit values of x_1, fractional Cu(1) site occupancies for dopant. Results are given based on analysis of the (001) peak, the (004) peak, and both peaks together. Uncertainties in x_1 are estimated to be consistent with the standard deviations of the data point as described in the text. The Co ($x=0.2$) sample has undetermined uncertainty for the (004) peak because the number of data points taken (2) is equal to the number of parameters used in the fit.

Sample	x_1 (001)	x_1 (004)	x_1
Fe ($x=0.3$)	0.85 ± 0.09	0.85 ± 0.15	0.85 ± 0.11
Fe ($x=0.5$)	0.76 ± 0.06	0.72 ± 0.07	0.75 ± 0.06
Co ($x=0.2$)	1.10 ± 0.07	$0.93\pm\ldots$	1.04 ± 0.05
Co ($x=0.5$)	0.82 ± 0.07	0.72 ± 0.08	0.78 ± 0.07
Ni ($x=0.3$)	0.40 ± 0.07	...	0.40 ± 0.07
Zn ($x=0.3$)	0.29 ± 0.08	...	0.29 ± 0.08

We first studied the sensitivity of the optimal dopant site occupancy to oxygen content, using the Co ($x=0.5$) and Ni ($x=0.3$) samples. The oxygen concentrations of the samples as measured by iodometric titration are 6.99 and 6.97, respectively, and give results of $x_1=0.78$ and 0.42. We examined the effect on optimal x_1 for each sample when the oxygen contents of the models were changed by ±0.2, a quantity substantially larger than the uncertainty in the titration measurement. The total oxygen content of the model was changed via the oxygen occupancies in the planes containing the Cu(1) sites. For the Ni-doped sample, we found that the results remain unchanged by either lowering or raising the oxygen content of the model by 0.2 oxygen atoms per unit cell. The re-

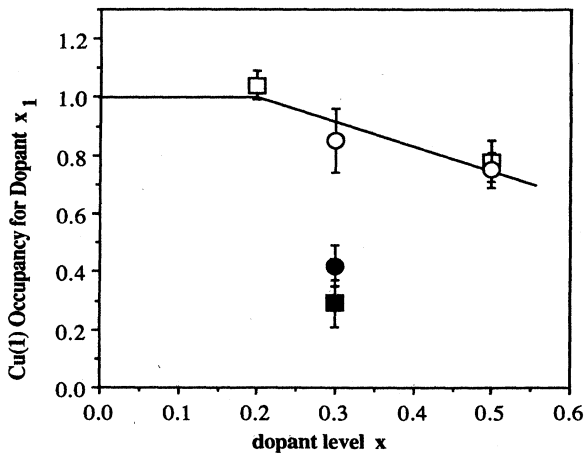

FIG. 10. Fraction of dopant on the Cu(1) site vs dopant level. Fe results are shown in open circles, Co results in open squares, Ni results in closed circle, and Zn results in closed square. Note that the samples fall into two categories: Fe and Co, which remain on the Cu(1) site at low x, gradually beginning to occupy the Cu(2) site as x increases, in contrast with Ni and Zn, which show essentially no site preference at $x=0.3$.

TABLE II. The ratios of quality-of-fit measures R to the best-fit value of R when data is fit to the $x_1=1.00$ (all chains) model, the $x_1=0.33$ (random) model, and the $x_1=0.00$ (all planes) model.

Sample	$R(x_1=1.00)$	$R(x_1=0.33)$	$R(x_1=0.00)$
Fe ($x=0.3$)	12.5	188.3	603.5
Fe ($x=0.5$)	33.1	170.2	720.3
Co ($x=0.2$)	1.2	59.4	140.2
Co ($x=0.5$)	16.4	109.7	464.3
Ni ($x=0.3$)	87.6	3.7	84.8
Zn ($x=0.3$)	159.2	1.8	86.1

sults for the Co-doped sample increased to $x_1=0.82$ for the oxygen concentration of 6.79, and decreased to $x_1=0.74$ for the oxygen concentration of 7.19, just within the error bars of the original answer. Thus, we conclude that our results are relatively insensitive to the total oxygen content assumed in the modeling.

Second, we examined the sensitivity of the results to total dopant concentration. The (003) and (113) reflections have been shown to be independent of the distribution of the dopant between the two Cu sites; therefore, the size of the knee in the energy dependence of the intensity at the dopant absorption edge is a function of the total dopant concentration for these reflections. This is illustrated in a comparison of the (003) or (113) curves of the lower and higher concentrations of Fe- or Co-doped Y-Ba-Cu-O. In principle, the total dopant concentration can be checked by fitting the total dopant concentration to the (003) and (113) data. In practice, however, for large changes in the total dopant concentration, the relative intensity changes on a scale comparable to that of the uncertainty in the data, so the technique is not always useful as an independent verification of the total dopant concentration.

How sensitive the results are to changes in total dopant concentration depends on the results themselves. When the dopants are unequally distributed between the Cu(1) and Cu(2) sites, as in the Fe- and Co-doped samples, the energy dependence of the intensities of the (001) and (004) reflections is strong. Then if a lower total dopant concentration is assumed, the models are able to compensate by creating a more unequal distribution between x_1 and x_2. On the other hand, when the dopants are about equally distributed among the sites ($x_1\approx 0.33$), the energy dependence of the (001) and (004) peaks is much weaker. Thus the derived distribution of Ni or Zn dopants is less sensitive to total dopant concentration. In all cases, the ability to distinguish among different values of x_1 diminishes with decreasing dopant concentration.

For the Ni- and Zn-doped samples, determining the sensitivity of our results to a reduction in the total dopant concentration is particularly important because the impurity phases observed in the x-ray powder-diffraction patterns could contain some Ni or Zn. We believe that most of the dopant is present in the $YBa_2Cu_3O_{7-\delta}$ phase, from observed changes in lattice parameters and suppression of T_c. However, EXAFS studies of a Ni ($x=0.3$) sample virtually identical to ours have suggested that about one-third of the Ni appears to be in a contaminating phase with features very similar to those of NiO.[19] Other researchers have also reported contamination by NiO and their EXAFS spectra of Ni-doped Y-Ba-Cu-O.[20,21] This NiO could possibly exist as clusters too small to give rise to sharp Bragg peaks, thus remaining undetected by x-ray powder diffraction.

Choosing the Co ($x=0.5$), the Ni ($x=0.3$), and the Zn ($x=0.3$), samples, we studied the effects on optimal x_1 when the total dopant content is changed. For the Ni-doped sample, the fraction of dopant on the Cu(1) site remained at 0.42 for a 10% increase or decrease in total dopant concentration. When the dopant concentration was reduced to $x=0.2$, the optimal Cu(1) site occupancy decreased only slightly from 0.42 to 0.37. At the same time, the fit to the (003) peak was improved insignificantly. For the Zn-doped sample, reduction of the total dopant concentration to $x=0.2$ caused the optimal x_1 to decrease from 0.29 to 0.23, an answer within the uncertainty of the original result. In this case, the fit to the (003) peak was degraded insignificantly. As predicted, the Co-doped sample showed more sensitivity to the total dopant concentration. When the total dopant concentration was decreased by 10%, the optimal Cu(1) site occupancy increased to $x_1=0.81$; when the total dopant concentration was reduced by 10%, x_1 decreased to 0.76. Even with the Co-doped samples, the optimal Cu(1) site occupancies remained within the error bars of the original answers, so we conclude that the results stand up to small changes in total dopant concentration.

Conceptually, a study of the sensitivity of the results to small changes in the anomalous corrections to the atomic scattering factor (f' and f'') of the dopant is similar to the study of the effects of changing the total dopant concentration, described above. If the magnitude of the differential intensity increases with the total dopant content, it will also increase with the magnitude of the correction to the atomic scattering factor. As with total dopant content, samples with an unequal distribution of dopant atoms will be more affected by changes in f' and f''; thus the Fe- and Co-doped samples should be more sensitive than the Ni- and Zn-doped samples. In fact, we found that the same result obtained for the Ni-doped sample when free-atom calculations of f' and f'' were used instead of the experimentally determined values, even though for the higher energies, differences in f' on the order of 1 electron occurred. In contrast, when we used the free-atom values for the Co ($x=0.5$) sample (Fig. 2), the fraction of Co atoms occupying the Cu(1) site decreased from 87 to 62%. Part of this greater sensitivity was due to the fact that for the energies used for Co, the difference in free atom and experimental anomalous corrections was 4 electrons at the highest energy. This result is well outside the uncertainty of our original result, although it still indicates Co's strong preference for the Cu(1) site. In this case the R value of the best fit to the free-atom model was nearly two orders of magnitude worse than when the experimental values were used for f' and f''.

Finally, a measure of the sensitivity of the results to variations in the relative atomic coordinates can be seen by comparing the results for the Co ($x=0.5$), Fe ($x=0.5$), and Zn ($x=0.3$) samples, in changing from the undoped Y-Ba-Cu-O coordinates with appropriate lattice parameters and symmetrized oxygen occupancies, to coordinates determined by neutron diffraction of doped Y-Ba-Cu-O.[13,14,16] For the Co ($x=0.5$) sample, the optimal Cu(1) site occupancy for Co increases only slightly in changing from undoped to doped coordinates, from $x_1=0.77$ to $x_1=0.78$. When the result is broken down into the separate (001) and (004) results, the agreement between them can be examined. For the (001) result, x_1 increases from 0.80 to 0.82, while for the (004) result, x_1 decreases from 0.73 to 0.72 when the doped coordinates are used. Thus, in the Co($x=0.5$) case, results using doped or undoped relative coordinates are very similar. This does not hold for the Fe ($x=0.5$) case. For the Fe ($x=0.5$) sample, the optimal Cu(1) site occupancy for Fe decreases only slightly, from 0.75 to 0.73, in replacing the undoped coordinates with coordinates derived from doped material. However, the agreement between the result based on the (001) reflection and that based on the (004) reflection worsens considerably when the doped coordinates are introduced. The (001) reflection alone gives $x_1=0.82$, while the (004) reflection gives $x_1=0.67$, and the error bars of the two results no longer overlap. [For the Fe ($x=0.3$) sample, for which shifts from the undoped coordinates are smaller, adjustment of the coordinates does not change the results.] The poor agreement between the (001) and (004) results when the doped coordinates are used is consistent with the fact that the sample from which they were derived differed significantly from ours, as discussed earlier. We believe that the results based on the undoped coordinates are more applicable for our Fe-doped samples. For comparison, we also examined the sensitivity to variations in relative coordinates for the Zn-doped sample. When the doped coordinates were replaced with undoped coordinates, x_1 was found to increase from 29 to 31%.

DISCUSSION

Our results demonstrating that Ni and Zn dopants distribute themselves approximately equally among the Cu sites are the first statistically significant results for Ni- and Zn-doped Y-Ba-Cu-O. In addition, our assignments of Cu site occupancies for Fe and Co confirm previous results while increasing their accuracy.

Neutron-diffraction studies of Zn-doped Y-Ba-Cu-O,[14,22] Ni-doped Y-Ba-Cu-O,[22] Co-doped Y-Ba-Cu-O,[23,24] and Fe-doped Y-Ba-Cu-O (Refs. 16, 17, and 25) have been published. The first neutron-diffraction study of Zn-doped Y-Ba-Cu-O was interpreted as showing that Zn occupies only Cu(2) sites, although up to 33% occupation of the Cu(1) site by Zn (i.e., random) could not be ruled out statistically.[14] Because they report a more substantial T_c suppression than was evident in our samples, materials differences may account for some of the discrepancy. Nevertheless, their uncertainty is large enough to include our result. The second neutron-diffraction study of Zn-doped Y-Ba-Cu-O gives results apparently contradicting ours, finding that $\frac{2}{3}$ of the Zn atoms occupy the Cu(1) site for $x=0.3$.[22] The same group studied Ni-doped Y-Ba-Cu-O and found that Ni dopants occupy only the Cu(2) site for $x=0.2$. These discrepancies may also arise from a difference in materials preparation, evidenced by both samples having lower oxygen contents and lower T_c's. Also, since no statistical evaluation of the fits is given in either case, their uncertainties may be large enough that their results overlap ours.

Neutron powder diffraction of Co-doped Y-Ba-Cu-O (Ref. 23) on samples virtually identical to those used in our experiment has shown that at $x=0.2$, all Co atoms occupy the Cu(1) site, in strict agreement with our results. The same group found that Co ($x=0.8$) produced a Cu(1) occupancy of 89%, whereas we found a larger fraction of Co atoms on the Cu(2) site at a lower Co concentration, $x_1=(78\pm4)\%$ for a dopant concentration of $x=0.5$. Qualitatively the results agree, and again, the uncertainty of the neutron results may be large enough to overlap our results. Another neutron-diffraction study of Co ($x=0.84$) found that Co substitutes into the Cu(1) site only,[24] a result clearly different from an extrapolation of our results. In addition, three neutron-diffraction studies have appeared in the literature on Fe-doped Y-Ba-Cu-O. Two of the three find that at low concentrations, $x=0.1$ (Ref. 25) and $x=0.23$,[16] Fe occupies the Cu(1) site exclusively. A third study of Fe ($x=0.15$) (Ref. 17) shows that 20% of the Fe atoms occupy the Cu(2) site, a higher occupancy than would be extrapolated from our results. In many of these cases, differences in sample preparation make direct comparison with our results difficult.

EXAFS has been used to probe the local environment of the transition-metal dopant for Fe- and Co-doped Y-Ba-Cu-O (Ref. 26) using samples virtually identical to samples used in this study. Both dopants were found to have distorted local environments with oxygen coordinations averaging between that of the square-planar Cu(1) atoms and that of the square-pyramidal Cu(2) atoms in the undoped material. Furthermore, the second-nearest-neighbor peaks of the EXAFS spectra are interpreted as showing that dopants are displaced within the *a-b* planes from the Cu sites, and perhaps ordered within the planes as well. Displacements within the *a-b* planes will not affect the intensities of the peaks examined in our experiment, and perpendicular distortions that affect the relative atomic coordinates are automatically included. EXAFS experiments, which give information about the local structural and chemical environment, are complementary to the DAS experiments, which give information about the average site occupancies of the dopant. Since the local structures are modified from the undoped structure by the presence of the dopant, they do not determine the site distributions within the lattice directly.

Mössbauer spectroscopy has also been used to probe the local environment of the Fe atom in Fe-doped Y-Ba-Cu-O.[27–32] Most of these studies show three different local environments for the Fe dopant as well as a dependence upon the total concentration of Fe. Depending upon the

interpretation of the spectra, various site distributions can be made consistent with the Mössbauer data. A prevalent interpretation is that Fe occupies the Cu(1) site exclusively at low x, then begins to occupy the Cu(2) site as x increases. Our results are consistent with such a mixed-site interpretation.

Previous thermogravimetric analyses (TGA) of transition-metal-doped Y-Ba-Cu-O give results consistent with those presented here. Since extra oxygen is much more easily accommodated in the Cu(1) plane,[33-35] an observation that oxygen is less easily removed from (or taken up by) a doped compound indirectly indicates that the Cu(1) site has been affected. The ease of oxygen removal from Ni- or Zn-doped Y-Ba-Cu-O is found comparable to that of the undoped material.[9] This observation suggests that neither Ni nor Zn perturbs the oxygen sites surrounding Cu(1), but since neither dopant introduces additional oxygen to the sample, no new information is gained by TGA about the site occupancy for Ni- or Zn-doped Y-Ba-Cu-O. On the other hand, the oxygen content of Fe- and Co-doped Y-Ba-Cu-O increases with x.[9,36] In this case, TGA studies find that oxygen remains trapped upon Co or Fe doping.[9] Therefore, TGA studies provide consistent albeit indirect evidence that Fe and Co primarily dope the Cu(1) site.

Measurements of the Hall constant have been published for Ni- and Co-coped Y-Ba-Cu-O, samples virtually identical to the samples studied here.[37,38] A distinctive property of high-temperature superconductors is that the Hall effect is strongly temperature dependent. Doping Y-Ba-Cu-O with Ni or Co suppresses this temperature dependence. In the regime of $x > 0.3$, Hall-derived estimates of the number of carriers might be meaningful. Motivated by this possibility, Clayhold and co-workers[37,38] examined the Hall coefficients and found a striking difference in magnitude between the Ni and Co cases. These results were interpreted on the basis that the formal valence of the Cu atoms is the same as comparable samples without Ni or Co. Our results show that at x close to 0.3, about a third of the Ni is on the Cu(1) site and a significant fraction of Co is on the Cu(2) site. To be consistent with their interpretation, Cu must be formally +2 on the Cu(1) site, and the formal charge of Co on the Cu(2) site must be +2 or compensated by oxygen.

We also examined whether the distribution of dopant atoms between the Cu sites is correlated with the superconducting critical temperature. The form of the variation of T_c with dopant concentration classifies Ni with Zn and Fe with Co,[9,36,39-44] and we have found a similar classification based on the distribution of the dopant atoms within the unit cell. However, no simple correlation exists between T_c and the amount of dopant on either the Cu(1) or the Cu(2) site individually. To investigate this further, we calculated the average nearest-neighbor distance to a dopant atom in the Cu(2) plane, assuming dopants randomly distributed therein. The results are listed in Table III. A range of values is given for the Ni- and Zn-doped samples to encompass the results when the amount of dopant in the $YBa_2Cu_3O_{7-\delta}$ phase is between $x=0.2$ and $x=0.3$. A possible interpretation of these results is that T_c is suppressed faster when Fe or Co atoms populate the Cu(2) site instead of Ni or Zn. Further experiments to compare more dopant concentrations would help clarify this point. The T_c suppression in Fe- and Co-doped Y-Ba-Cu-O does not seem consistent with a BCS-type magnetic pair-breaking mechanism because the degree of T_c suppression is not linear with dopant concentration and is much weaker than that seen in traditional superconductors with magnetic impurities. Furthermore, some evidence that Ni is magnetic in Y-Ba-Cu-O has appeared in the literature.[9]

TABLE III. Average nearest-neighbor distances to a dopant atom in the Cu(2) plane. This number is calculated by assuming a discrete lattice with random distribution of the dopant atoms throughout the a-b plane. For reference, T_c data are also listed. For the Ni- and Zn-doped samples, ranges of distances are given to encompass total dopant concentrations in the $YBa_2Cu_3O_{7-\delta}$ phase of $x=0.2$ to $x=0.3$.

Sample	d (Å)	T_c (K)[a]
Fe ($x=0.3$)	21.1	40
Fe ($x=0.5$)	13.4	0
Co ($x=0.2$)	...	53
Co ($x=0.5$)	13.8	0
Ni ($x=0.3$)	11–13	40
Zn ($x=0.3$)	10–12	45

[a] J. M. Tarascon *et al.*, Phys. Rev. B **37**, 7458 (1988).

Finally, we have demonstrated that anomalous x-ray-scattering techniques can be a sensitive and generally applicable probe of the cation distribution in these multicomponent crystalline materials. Additional studies to test for ordering within the layers, to examine the possibility of cation disorder among Y, Ba, and Cu or to look at other related systems are possible with extensions of this technique.

ACKNOWLEDGMENTS

We thank J. Boyce, F. Bridges and T. Claeson for the use of their absorption data of Ni- and Zn-doped Y-Ba-Cu-O. In addition, we thank Rick Trebino for helpful discussions of statistical analysis, Bob Smith for technical assistance, and Sean Brennan for assistance with Stanford Synchrotron Radiation Laboratory (SSRL) software. This work was supported in part by the Air Force Office of Scientific Research under Contract No. F49620-88-C-0004, and work at SSRL was supported by the U.S. Department of Energy under Contract No. DE-AC03-82ER-1300, Office of Basic Energy Sciences, Division of Chemical Sciences, and the National Institutes of Health, Biotechnology Resource Program, Division of Research Resources.

[1]Y. LePage, W. R. McKinnon, J. M. Tarascon, L. H. Greene, G. W. Hull, and D. M. Hwang, Phys. Rev. B **35**, 7115 (1987).
[2]J. E. Greedan, A. O'Reilly, and C. V. Stager, Phys. Rev. B **36**, 8770 (1987).
[3]M. A. Beno, L. Soderholm, D. W. Capone II, D. G. Hinks, J. D. Jorgensen, J. D. Grace, I. K. Shuller, C. U. Segre, and K. Zhang, Appl. Phys. Lett. **51**, 57 (1987).
[4]J. J. Capponi, C. Chailout, A. W. Hewat, P. Lejay, M. Marezio, N. Nguyon, B. Raveau, J. L. Soubeyroux, J. L. Tholence, and R. Tournier, Europhys. Lett. **3**, 1301 (1987).
[5]W. I. F. David, W. T. A. Harrison, J. M. F. Gunn, O. Moze, A. K. Soper, P. Day, J. D. Jorgensen, M. A. Beno, D. W. Capone II, D. G. Hinks, I. K. Schuller, L. Soderholm, C. U. Segre, K. Zhang, and J. D. Grace, Nature **327**, 310 (1987).
[6]F. Beech, S. Miraglia, A. Santoro, and R. S. Roth, Phys. Rev. B **35**, 8778 (1987).
[7]S. Katano, S. Funahashi, T. Hatano, A. Matsushita, K. Nakamura, T. Matsumoto, and K. Ogawa, Jpn. J. Appl. Phys. **26**, L1046 (1987).
[8]P. H. Fuoss, P. Eisenberger, W. K. Warburton, and A. Bienenstock, Phys. Rev. Lett. **46**, 1537 (1981).
[9]J. M. Tarascon, P. Barboux, P. F. Miceli, L. H. Greene, G. W. Hull, M. Eibschutz, and S. A. Sunshine, Phys. Rev. B **37**, 7458 (1988).
[10]W. Parrish, M. Hart, and T. C. Huang, J. Appl. Crystallogr. **19**, 92 (1986).
[11]M. S. Jensen, J. Phys. B **13**, 4337 (1980).
[12]D. T. Cromer and D. Liberman, J. Chem. Phys. **53**, 1891 (1970).
[13]P. F. Miceli (private communication).
[14]Gang Xiao, M. Z. Cieplak, D. Musser, A. Gavrin, F. H. Streitz, C. L. Chien, J. J. Rhyne, and J. A. Gotaas, Nature **332**, 238 (1988).
[15]Y. K. Tao, J. S. Swinnea, A. Manthiram, J. S. Kim, J. B. Goodenough, and H. Steinfink, J. Mater. Res. **3**, 248 (1988).
[16]P. Bordet, J. L. Hodeau, P. Strobel, M. Marezio, and A. Santoro, Solid State Commun. **66**, 435 (1988).
[17]G. Roth, G. Heger, B. Renker, J. Pannetier, C. Caignaert, M. Hervieu, and B. Raveau, Physica C. **153-155**, 972 (1988).
[18]P. R. Bevington, *Data Reduction and Error Analysis for the Physical Sciences* (McGraw-Hill, San Francisco, 1969), p. 314.
[19]F. Bridges (private communication).
[20]M. Qian, E. A. Stern, Y. Ma, R. Ingalls, M. Sarikaya, B. Thiel, R. Kurosky, C. Han, L. Hutter, and I. Aksay (unpublished).
[21]K. Zhang, G. Bunker, and B. Chance (unpublished).
[22]T. Kajitani, K. Kusaba, M. Kikuchi, Y. Shono, and M. Hirabayashi, Jpn. J. Appl. Phys. **27**, L354 (1988).
[23]P. F. Miceli, J. M. Tarascon, L. H. Greene, P. Barboux, F. J. Rotella, and J. D. Jorgensen, Phys. Rev. B **37**, 5932 (1988).
[24]P. Zolliker, D. E. Cox, J. M. Tranquada, and G. Shirane, Phys. Rev. B **38**, 6575 (1988).
[25]X. Obradors, M. Vallet, J. Rodriguez, J. Fontcuberta, A. Labarta, and J. M. Gonzalez-Calbet, Physica C **153-155**, 888 (1988).
[26]F. Bridges, J. B. Boyce, T. Claeson, T. H. Geballe, and J. M. Tarascon (unpublished).
[27]M. Takano, Z. Hiroi, H. Mazaki Y. Bando, Y. Takeda, and R. Kanno, Physica C **153-155**, 860 (1988).
[28]H. U. Krebs, O. Bremert, and C. Michaelson, Physica C **153-155**, 966 (1988).
[29]O. Bremert, C. Michaelsen, and H. U. Krebs (unpublished).
[30]T. Tamaki, T. Komai, A. Ito, Y. Maeno, and T. Fujita, Solid State Commun. **65**, 43 (1987).
[31]H. Tang, Z. Q. Qiu, Y.-w. Du, Gang Xiao, C. L. Chien, and J. C. Walker, Phys. Rev. B **36**, 4018 (1987).
[32]Z. Q. Qiu, Y. W. Du, H. Tang, J. C. Walker, W. A. Bryden, and K. Moorjani, J. Magn. Mater. **69**, L221 (1987).
[33]J. M. Tarascon, P. Barboux, B. G. Bagley, L. H. Greene, W. R. McKinnon, and G. W. Hull, in *Chemistry of High Temperature Superconductors,* edited by D. L. Nelson, M. S. Whittingham, and T. F. George, ACS Symposium Series, No. 351 (American Chemical Society, Washington, DC, 1987), p. 198.
[34]J. D. Jorgensen, M. A. Beno, D. G. Hinks, L. Soderholm, K. J. Volin, R. L. Hitterman, J. D. Grace, I. K. Schuller, C. U. Segre, K. Zhang, and M. S. Kleefisch, Phys. Rev. B **36**, 3608 (1987).
[35]R. J. Cava, B. Batlogg, C. H. Chen, E. A. Rietman, S. M. Zahurak, and D. Werder, Phys. Rev. B **36**, 5719 (1987).
[36]J. F. Bringley, T.-M. Chen, B. A. Averill, K. M. Wong, and S. J. Poon, Phys. Rev. B **38**, 2432 (1988).
[37]J. Clayhold, N. P. Ong, Z. Z. Wang, J. M. Tarascon, and P. Barboux (unpublished).
[38]J. Clayhold, S. Hagen, Z. Z. Wang, N. P. Ong, J. M. Tarascon, and P. Barboux, Phys. Rev. B **39**, 777 (1989).
[39]T. Takabatake and M. Ishikawa, Solid State Commun. **66**, 413 (1988).
[40]M. Ishikawa, T. Takabatake, A. Tohdake, Y. Nakazawa, T. Shibuya, and K. Koga, Physica C **153-155**, 890 (1988).
[41]Y. Maeno, T. Tomita, M. Kyogoku, S. Awaji, Y. Aoki, K. Hoshino, A. Minami, and T. Fujita, Nature **328**, 312 (1987).
[42]Y. Maeno, M. Kato, Y. Aoki, and T. Fujita, Jpn. J. Appl. Phys. **26**, L1982 (1987).
[43]Gang Xiao, F. H. Streitz, A. Gavrin, Y. W. Du, and C. L. Chien, Phys. Rev. B **35**, 8782 (1987).
[44]Y. Maeno and T. Fujita, Physica C **153-155**, 1105 (1988).